Characterization of Vitrified Savannah River Site SB4 Waste Surrogate Produced in Cold Crucible

S.V. Stefanovsky
SIA Radon, Moscow, Russia

J.C. Marra
Savannah River National Laboratory, Aiken, SC, USA

A.A. Akatov
Institute of Technology, St-Petersburg, Russia

Keywords: Cold Crucible, Glass, Infrared Spectroscopy, Scanning Electron Microscopy, X-Ray Diffraction

Abstract

Savannah River Site (SRS) sludge batch 4 (SB4) waste surrogate with high aluminum and iron content was vitrified with commercially available Frit 503-R4 (8 wt.% Li_2O, 16 wt.% B_2O_3, 76 wt.% SiO_2) by cold crucible inductive melting using lab- (56 mm inner diameter), bench- (236 mm) and large-scale (418 mm) cold crucible. The waste loading ranged between 40 and 60 wt.%. The vitrified products obtained in the lab-scale cold crucible were nearly amorphous with traces of unreacted quartz in the product with 40 wt.% waste loading and traces of spinel phase in the product with 50 wt.% waste loading. The glassy products obtained in the bench-scale cold crucible are composed of major vitreous and minor iron-rich spinel phase whose content at ~60 wt.% waste loading may achieve ~10 vol.%. The vitrified waste obtained in the large-scale cold crucible was also composed of major vitreous and minor spinel structure phases. No nepheline phase has been found. Average degree of crystallinity was estimated to be ~12 vol.%. Anionic motif of the glass network is built from rather short metasilicate chains and boron-oxygen constituent based on boron-oxygen triangular units.

Introduction

Currently borosilicate glass is considered as a high level waste (HLW) form in the most of countries developing nuclear technologies. In the USA borosilicate glass has been chosen as a HLW form at the Defense Waste Processing Facility (DWPF) [1], where the HLW vitrification process is performed in a Joule Heated Ceramic Melter (JHCM). A cold crucible initially developed for production of high-fusible and high-pure single crystals, polycrystalline ceramics and glasses is considered as an alternative to the JHCM. Major advantages of the cold crucible over the JHCM are higher productivity, higher temperature availability, longer lifetime, smaller dimensions, and higher waste loading at the same product quality. Active hydrodynamic regime in the cold crucible prevents segregation of crystalline phases normally formed under stationary conditions in the crucibles heated in a resistive furnace.

Vitrification of high-ferrous sludge batch 2 (SB2) HLW surrogate yielded high-quality glassy material that contained minor spinel structure phase. The presence of the spinel phase did

negatively influence the chemical durability of the material [2]. In the present work we investigated in details phase composition, structure and chemical durability of the vitrified SB4 HLW surrogate with high iron and aluminum content.

Experimental

The tests on vitrification of SB4 waste surrogate (Table 1) were performed in:

- a lab-scale unit with a 56 mm inner diameter copper cold crucible with melt surface area of 24.6 cm^2 energized from a 5.28 MHz/10 kW generator [3];
- a bench-scale cold crucible facility using a 236 mm inner diameter cold crucible manufactured from stainless steel pipes and energized from a 1.76 MHz/60 kW generator [4];
- the Radon full-scale vitrification plant with a 418 mm inner diameter stainless steel cold crucible energized from a 1.76 MHz/160 kW generator [5].

The external surface of the crucibles was coated with ground fireclay based putty. Melting runs were described in details in ref. [3-5].

Table 1. Target and Actual Chemical Compositions (wt.%) of the SB4 Waste, Vitrified Waste Products Sampled from Canisters and the "Dead Volume" of the Cold Crucible

Oxides	SB4 waste	Target at WL			Bench-scale at WL			Full-scale, canisters #					
		40	50	60	40[1]	50[1]	60[2]	6,[2]	12,[2]	16,[2]	16,[1]	20,[2]	DV[2]
Li_2O	-	4.80	4.00	3.20	4.40	3.16	3.00	4.00	4.00	4.00	3.53	4.00	4.00
B_2O_3	-	9.60	8.00	6.40	11.50	8.72	6.70[3]	6.70	5.50	6.00	7.17	5.50	4.98
Na_2O	18.71	7.48	9.35	11.23	10.20	13.60	12.17	9.27	10.05	9.63	9.76	10.04	9.38
MgO	2.77	1.11	1.39	1.66	0.85	1.20	1.59	1.49	1.65	1.67	1.44	1.71	1.65
Al_2O_3	25.49	10.20	12.75	15.29	9.96	12.40	16.00	13.96	14.11	13.47	13.90	14.11	14.02
SiO_2	2.71	46.68	39.36	32.03	45.50	37.35	33.13	41.16	41.33	39.19	43.00	40.09	41.91
P_2O_5	-	-	-	-	-	-	-	0.09	0.12	0.08	0.08	0.12	0.12
SO_3	0.87	0.35	0.43	0.52	0.20	0.29	0.35	0.15	0.18	0.13	0.06	0.23	0.21
Cl	-	-	-	-	-	-	-	0.32	0.41	0.27	0.30	0.41	0.22
K_2O	0.07	0.03	0.03	0.04	0.04	0.04	0.04	0.08	0.08	0.08	0.10	0.09	0.07
CaO	2.77	1.11	1.38	1.66	2.05	3.36	2.55	1.64	1.58	1.76	1.52	1.49	1.41
TiO_2	0.04	0.01	0.02	0.02	0.02	0.02	0.01	0.02	0.04	0.01	0.04	0.02	0.03
Cr_2O_3	0.20	0.08	0.10	0.12	0.10	0.11	0.13	0.12	0.12	0.12	0.11	0.12	0.13
MnO	5.78	2.31	2.89	3.47	2.02	2.60	3.48	2.47	2.47	3.04	2.85	2.55	2.69
Fe_2O_3	28.99	11.60	14.49	17.39	13.40	15.70	18.50	12.86	12.98	13.79	10.85	13.61	13.32
NiO	1.66	0.66	0.83	1.00	0.62	0.78	1.00	2.36	2.11	2.56	2.19	2.14	2.09
CuO	0.05	0.02	0.03	0.03	0.03	0.02	0.03	0.04	0.03	0.03	0.03	0.02	0.05
ZnO	0.05	0.02	0.02	0.03	0.04	0.03	0.03	2.58	2.44	2.84	2.42	2.42	2.26
ZrO_2	0.09	0.04	0.05	0.54	0.07	0.04	0.06	0.05	0.07	0.07	0.07	0.05	0.07
Cs_2O[4]	<0.01	-	0.22	-	-	-	0.24	0.24	0.25	0.32	0.18	0.29	0.29
BaO	0.07	0.03	0.03	0.04	0.02	0.01	0.04	0.03	0.02	0.03	0.10	0.02	0.10
La_2O_3	0.03	0.01	0.02	0.02	<0.01	<0.01	0.02	0.03	0.02	0.03	0.01	0.05	0.07
Ce_2O_3	0.21	0.09	0.11	0.13	0.08	0.10	0.14	0.14	0.16	0.16	0.01	0.14	0.16
PbO	0.38	0.15	0.19	0.23	0.13	0.15	0.20	0.15	0.14	0.20	0.16	0.16	0.16
ThO_2[5]	0.03	0.01	0.02	0.02	-	-	-	-	-	-	-	-	-
U_3O_8[5]	9.03	3.61	4.52	5.42	-	-	-	-	-	-	-	-	-
Total	100.00	100.00	100.00	100.00	101.23	99.68	99.41	99.95	99.86	99.48	99.89	99.38	99.39

[1] determined by ICP-AES at SRNL, [2] determined by XRF at Radon, [3] determined by potentiometric titration,
[4] introduced over 100 wt.%,[5] ThO_2 and U_3O_8 were introduced only in the feed at the lab-scale tests.

Frit 503-R4 with chemical composition (wt.%) 8 Li_2O, 16 B_2O_3, SiO_2 was found based on laboratory testing at the Savannah River National Laboratory (SRNL) to be a suitable glass formulation when combined with the SB4 waste vitrification to obtain a nepheline free glassy material containing minor spinel structure phase [6]. Preliminary testing on preparation of the glass in an alumina crucible in a resistive furnace has shown that uniform glassy product is obtained at a temperature of 1300 °C. At lower temperatures the glassmelt was too viscous and inhomogeneous.

The durability data showing normalized release values for B, Li, Na and Si were obtained using glass samples from crucible-scale tests and performing PCT-A [7] on these glasses (Table 2). Data are also included for glass samples subjected to the Canister Centerline Cooling Profile (CCC) [8]. Both the glasses at 50 and 55 wt.% waste loading are quite chemically durable but the glass with 55 wt.% waste loading showed a slight decrease in durability under CCC conditions (Table 2). Thus the selection was made in favor of the glass with 50 wt.% waste loading.

Table 2. PCT-A [7] Data for Frit 503-R4 with Various Sludge Loadings

Glass ID	Waste Loading, wt.%	Normalized Release (g/L)			
		B	Li	Na	Si
503-R4	40	0.50	0.63	0.35	0.33
	45	0.41	0.52	0.35	0.32
	50	0.55	0.68	0.53	0.34
	55	0.42	0.56	0.53	0.34
503-R4 CCC	40	0.45	0.63	0.35	0.34
	45	0.41	0.52	0.35	0.32
	50	0.33	0.48	0.34	0.28
	55	0.59	0.75	0.49	0.32
SB4-40 (bench-scale)	40	0.28	0.48	0.36	0.26
SB4-50 (bench-scale)	50	0.48	0.60	0.65	0.28
SB4-60 (bench-scale)	60	0,66	0,71	0,57	0,32
SB4-50 (large-scale)	50	1,00	0,90	0,60	0,34
Environmental Assessment (EA) Standard		18.57	9.91	13.73	3.92
Approved Reference Material (ARM) Standard		0.48	0.56	0.48	0.26

In order to evaluate the effect of waste loading on the glass structure and elemental leaching, the waste loading in glass was varied from 40 to 60 wt.%.

In the lab-scale tests, vitrification was performed by rising melt level method and the glass specimens were sampled from the breakage removed from the cold crucible after its cooling to room temperature. At the bench- and full-scale tests, molten glass was periodically poured into 10 L canisters and annealed to relax mechanical stress. After cooling, glass in some canisters was cracked and the specimens were sampled from glass breakage.

In the full-scale test, 30 canisters with vitrified waste surrogate were obtained and specimens from canisters ## 6, 8, 10, 12, 14, 16, 18, 20, 21, 22 and “dead volume” of the cold crucible were sampled. All the specimens were glass-like, dark-colored, opaque and visually uniform. Chemical compositions of the glassy products sampled from canisters ## 6, 12, 16, 20 and from the “dead volume” were determined and compared with the target composition (Table 1).

The products were analyzed by X-ray fluorescence (XRF) spectroscopy using a PW-2400 Philips Analytical BV unit equipped with quantitative analytical Philips SuperQuantitative & IQ-2001 Software and Inductively Coupled Plasma – Atomic Emission Spectroscopy (ICP-AES) at SRNL. The vitrified products were examined by X-ray diffraction using a DRON-4

diffractometer (Fe Kα – radiation, scan range of 10 to 90 ° 2-θ), scanning electron microscopy with energy dispersive spectroscopy (SEM/EDS) using a JSM-5300 + Link ISIS unit (voltage is 25 KeV, beam current is 1 nA, probe diameter is 1 to 3 μm, dwell time is 100 s; metals, oxides and fluorides were used as standards). Infra-red spectra were recorded using an IKS-29 spectrophotometer (compaction of powdered glass in pellets with KBr). Chemical durability of the glassy products was determined using a PCT-A procedure [7].

Vitrified Product Characterization

Analytical data exhibit good conformity with the target glass composition with the exception of few elements. Shortfall in B_2O_3, SO_3, Cl, Cs_2O, PbO, and, to a less extent Na_2O, in the glasses produced in the large-scale cold crucible was due likely to their volatilization at high temperatures in the CCIM process, whereas excess of NiO and ZnO may be explained by their impurities in some chemicals used. In the whole all the analytical sums are close to 100 wt.%.

The material with 40 wt.% waste loading produced in the lab-scale cold crucible was found to be completely amorphous (Fig. 1, *1*). Occurrence of quartz (major reflection at 3.33-3.34 Å) was due likely to traces of incompletely dissolved quartz (Fig. 1, *2,3*). XRD patterns demonstrated occurrence of the spinel structure phase in the glassy products at ≥50 wt.% waste loading (Fig. 1, *4-7*). Traces of spinel phase may have been present in the glassy material at 40 wt.% waste loading produced in the bench-scale cold crucible and cooled relatively slowly in a heat-insulated box (Fig. 1, *2*).

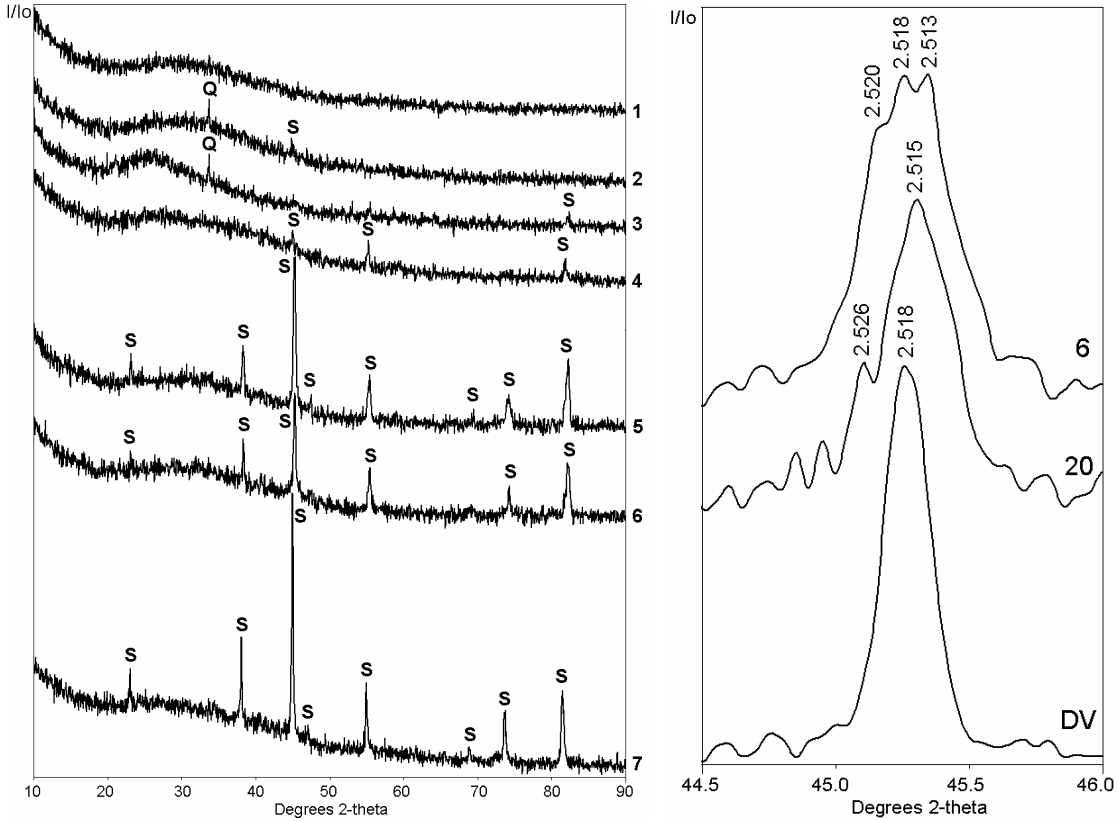

Figure 1. XRD Patterns of Glassy Materials at Waste Loadings of 40 (1,2), 50 (3-6) and 60 wt.% (7) Produced in the Lab- (1,3), Bench- (2,4,7), and Large-Scale (5,6) Cold Crucibles and Major Reflection due to Spinel in the Products Sampled from Canisters #6 and #20 and "Dead Volume". Q – quartz, S – spinel.

SEM/EDS study of the materials with ~50 wt.% waste loading produced in the lab- and bench-scale cold crucibles showed similarities in their microstructures. Primarily individual spinel crystals are distributed in a matrix vitreous phase (Fig. 2, *a*-*c*). Rare individual inclusions of unreacted quartz occurred (Fig. 2, *d*). No nepheline phase was found at even ~60 wt.% waste loading in glass produced in the bench-scale cold crucible and annealed in the heat-insulated box.

As follows from EDS data, partitioning of waste elements among vitreous and spinel type phases is typical of their crystal chemical behavior (Table 4): alkali (Na, K, Cs), alkali earth (Ca, Ba) elements, aluminum, silicon, sulfur, lead, and uranium are concentrated in the vitreous phase; transition elements (Cr, Mn, Fe, Ni, Cu, Zn) enter predominantly spinel. Some elements such as magnesium and cerium are distributed between both the phases.

Two glasses produced in the large-scale cold crucible were subjected to optical microscopy and three of the glasses were examined by SEM/EDS to study in more detail. In transmitted light, both the glasses are transparent, clear and brown colored in some areas. Spinel is black. Skeleton type spinel crystals are observed in the bulk (Fig. 3*a*). In the reflected light, the glass is gray-colored whereas the spinel is white or light-gray (Fig. 3*b*).

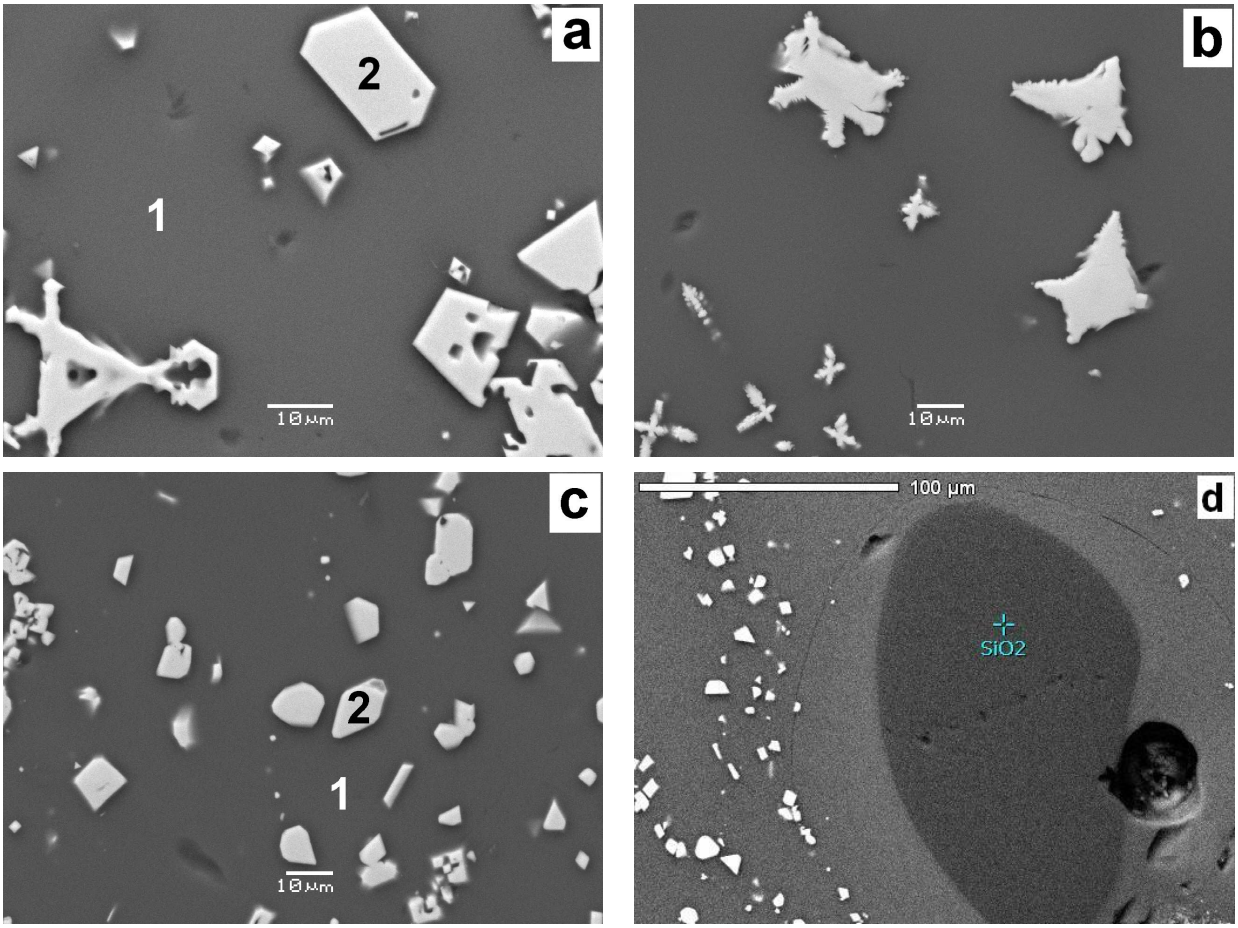

Figure 2. SEM images of the glassy materials with 50 (a, b) and 60 wt.% (c, d) waste loading produced in the lab- (a) and bench-scale (b-d) cold crucibles.1 – vitreous phase, 2 – spinel.

SEM images demonstrate non-uniform distribution of the spinel crystals in the bulk of the samples (Fig. 3*e*). The bulk consists of areas with different types of spinel crystals (Fig. 3*f*). Major bulk is composed of vitreous phase with the skeleton-type crystals up to several microns in size distributed within. These areas are separated by layers composed of matrix glass containing individual spinel crystals up to 20-30 μm in size (Fig. 4 *f-h*).

Occurrence of two different zones in the glass bulk may be due to non-uniform cooling rate of glass in canisters especially when two pours in the same canister were done. In this case interaction of hot melt with solidified melt in the canister creates temperature gradient forming zones with various cooling rates. Fast cooling results in crystallization of fine skeleton-type crystals whereas in the zones with slower cooling rate larger individual crystals were formed.

As follows from EDS measurements, chemical compositions of the vitreous phase and spinel in zones with different cooling rate are also varied especially in contents of microcomponents (Table 3). Major constituents of spinel are transition metal oxides (Fe, Mn, Ni, Cr, Zn) as well as alumina and magnesia. Such elements as Na, Si, K, Ca, Zr, Pb, and some Al and Mg were captured by electron probe from surrounding glass.

Table 3. Chemical Compositions (wt.%) of Co-Existing Phases in the Vitrified SB4 Waste

Oxides	Lab-scale		Bench-scale		Large-scale							
					Canister #6				Canister #20			
	Glass on Fig. 2*a*	Spinel on Fig. 2*a*	Glass on Fig. 2*c*	Spinel on Fig. 2*c*	Zone with skeleton-type crystals		Border zone with individual crystals		Zone of skeleton-type crystals		Zone of individual crystals	
					VF	Spinel	VF	Spinel	VF	Spinel	VF	Spinel
Na_2O	8.44	0.54	13.04	0.43	10.16	1.91	9.58	1.24	8.96	1.59	9.32	1.24
MgO	1.06	1.09	1.65	1.66	1.40	0.81	1.44	0.68	1.66	1.07	1.52	0.90
Al_2O_3	12.42	2.54	15.39	2.71	14.22	6.71	14.26	6.61	14.07	6.01	14.23	6.41
SiO_2	42.16	0.51	39.75	0.35	43.92	5.51	43.30	3.04	43.28	4.94	43.85	3.48
SO_3	0.43	0.11	0.18	0.13	-	0.00	0.20	0.05	0.00	0.05	0.07	0.00
K_2O	-	-	-	-	0.22	0.01	0.20	0.02	0.16	0.05	0.18	0.04
CaO	1.27	0.10	3.38	0.10	1.64	0.17	1.71	0.13	1.80	0.12	1.67	0.11
TiO_2	-	-	-	-	0.09	0.27	0.00	0.11	0.04	0.04	0.06	0.16
Cr_2O_3	0.08	3.47	0.05	1.80	0.12	1.47	0.07	8.01	0.13	2.51	0.05	3.65
MnO	3.20	5.52	2.86	5.43	2.63	1.80	2.79	2.09	2.75	1.69	2.95	1.86
Fe_2O_3	12.58	71.03	8.07	73.92	6.88	56.66	7.05	52.05	6.74	56.13	6.37	57.36
NiO	0.40	13.91	0.07	13.63	1.04	21.71	0.98	19.93	0.79	21.98	0.91	20.88
CuO	<0.01	0.02	<0.01	0.03	0.08	0.08	0.05	0.07	0.19	0.07	0.04	0.19
ZnO	<0.01	0.32	<0.01	0.14	3.38	3.36	3.37	4.61	4.04	3.00	3.83	3.75
ZrO_2	-	-	-	-	-	0.05	0.20	0.00	0.19	0.27	0.14	0.35
Cs_2O	0.15	<0.01	0.44	<0.01	0.29	-	0.39	-	0.43	0.00	0.40	0.00
BaO	<0.01	0.01	0.02	<0.01	-	0.06	0.00	0.00	0.17	0.00	0.00	0.00
La_2O_3	-	-	-	-	-	0.21	0.24	0.22	0.06	0.00	0.00	0.06
Ce_2O_3	0.08	0.32	0.22	0.27	0.12	0.19	0.25	0.26	0.05	0.22	0.12	0.00
PbO	<0.01	<0.01	0.15	<0.01	0.38	0.21	0.25	0.00	0.22	0.11	0.15	0.09
U_3O_8	4.83	<0.01	-	-	-	-	-	-	-	-	-	-
Total*	87.12	99.48	85.25	100.60	86.53	101.20	86.32	99.13	85.74	99.84	85.86	100.53

* oxide sums for analyses of vitreous phase are less than 100 wt.% because Li and B are not determined by EDS, VF – vitreous phase.

The spinel structure phase segregated as the skeleton-type crystals is close to magnetite in chemical composition and its average formula may be represented as ($Mg_{0.03}Mn_{0.07}Fe_{0.05}Ni_{0.76}$

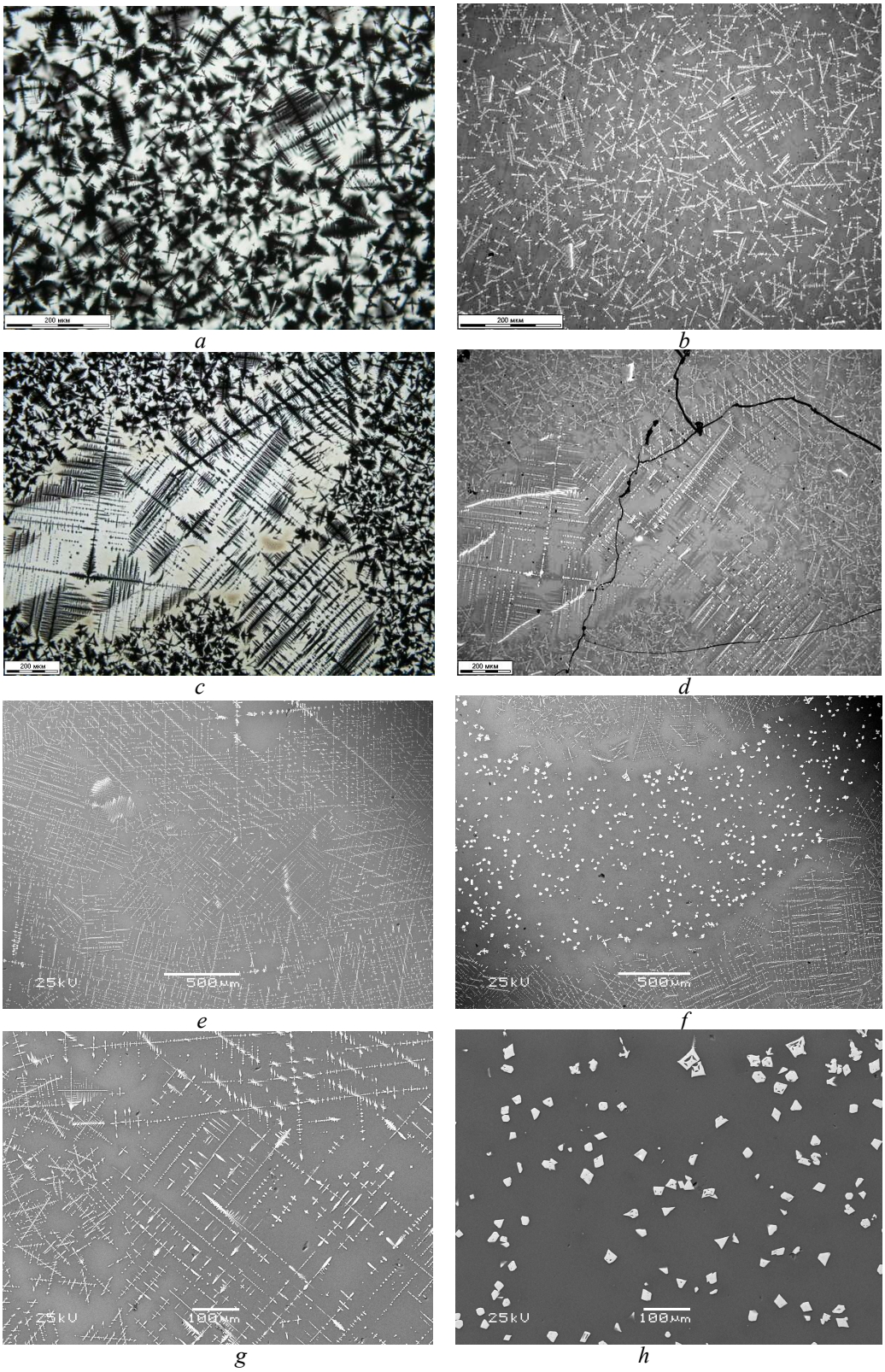

a *b* *c* *d* *e* *f* *g* *h*

Figure 3. Photomicrographs in Optical Microscope of the Samples from Canister #6 (a, b) and "Dead Volume" of the Cold Crucible (c, d) in Transmitted (a, c) and Reflected (b, d) Light at Parallel Nicols (scale bars are 200 µm) and SEM Images of the Glassy Product from Canister #6 (e – general view, f – border zone, g – zone of skeleton-type crystals, h – zone of individual crystals).

$Zn_{0.09})^{2+}(Fe_{1.76}Al_{0.19}Cr_{0.05})^{3+}O_4$ (Spinel-1). In the zone of individual crystals one of the varieties has a chemical composition similar to that in the zone of the skeleton-type crystals and formula $(Mg_{0.04}Mn_{0.07}Fe_{0.07}Ni_{0.73}Zn_{0.09})^{2+}(Fe_{1.81}Al_{0.16}Cr_{0.04})^{3+}O_4$ (Spinel-1). The second variety is enriched with chromium and, in some extent, with zinc and has a formula $(Mg_{0.02}Mn_{0.08}Fe_{0.11}Ni_{0.62}Zn_{0.17})^{2+}(Fe_{1.31}Al_{0.17}Cr_{0.52})^{3+}O_4$ (Spinel-2). Some grains have intermediate composition: $(Mg_{0.02}Mn_{0.07}Fe_{0.08}Ni_{0.69}Zn_{0.14})^{2+}(Fe_{1.58}Al_{0.16}Cr_{0.26})^{3+}O_4$ (Spinel-3). Based on SEM/EDS data the Spinel-1 variety may be identified as a trevorite (JCPDS-ICDD 44-1485 or 23-1119) and two others – as solid solutions between trevorite and zincochromite, $ZnCr_2O_4$ (JCPDS-ICDD 22-1107).

The glassy products from Canister #20 and "dead volume" of the cold crucible have a texture similar to that observed in the product from Canister #6. Both samples have zones with the skeleton-type crystal aggregates distributed in the glassy matrix and with larger-sized individual crystals (Fig. 4). Chemical compositions of the phases co-existing in the zones with the skeleton-type and individual crystals in the glassy product from Canister #20 are given in Table 3.

Like in the sample from Canister #6, we have good agreement between the target glass composition and composition of the vitreous phase in the samples from Canister #20. In both zones with the skeleton-type and individual crystals analytical sums of the vitreous phase constituents are about 84-87 wt.%. Taking into account that the target sum of Li_2O and B_2O_3 is 12 wt. (4 wt.% Li_2O + 8 wt.% B_2O_3) the total is about 96-99 wt.%. These results are very near the target considering that some minor anionic constituents (F, Cl, P) were not determined.

Formulae of the spinel phases in the sample from Canister #20 recalculated from their chemical compositions (Table 3) are as follows:

- in the zone of the skeleton-type crystals:
  $(Mg_{0.04}Mn_{0.06}Fe_{0.13}Ni_{0.77}Zn_{0.10})^{2+}(Fe_{1.71}Al_{0.15}Cr_{0.04})^{3+}O_4$ (Spinel-1),
  $(Mg_{0.03}Mn_{0.07}Fe_{0.09}Ni_{0.74}Zn_{0.07})^{2+}(Fe_{1.68}Al_{0.13}Cr_{0.19})^{3+}O_4$ (Spinel-2);
- in the zone with individual crystals:
  $(Mg_{0.04}Mn_{0.07}Fe_{0.08}Ni_{0.73}Zn_{0.08})^{2+}(Fe_{1.81}Al_{0.18}Cr_{0.01})^{3+}O_4$ (Spinel-1),
  $(Mg_{0.05}Mn_{0.07}Fe_{0.09}Ni_{0.71}Zn_{0.08})^{2+}(Fe_{1.64}Al_{0.14}Cr_{0.22})^{3+}O_4$ (Spinel-2),
  $(Mg_{0.01}Mn_{0.06}Fe_{0.14}Ni_{0.73}Zn_{0.06})^{2+}(Fe_{1.79}Al_{0.07}Cr_{0.14})^{3+}O_4$ (Spinel-3).

All the spinel varieties are cubic with a space group *Fd3m* (*Z*=8). Their lattice parameters determined from XRD data (Fig. 1) are given in Table 4. As seen from Fig. 1, major reflection on XRD pattern due to the spinel structure phase in the product sampled from Canister #6 is split into three peaks corresponding to three different spinel varieties. Significant asymmetry of the peak and occurrence of "shoulders" from both lower and higher angles of 2-theta demonstrate incomplete phase formation under non-equilibrium spinel crystallization conditions from the melt yielding spinel grains with variable chemical composition. Spinel grains in the product from

Table 4. Averaged Lattice Parameters of the Spinel Varieties in the Glassy Products

Product	Spinel	d_{max}, Å	*a*, Å
Canister #6	Spinel-2	2.520	8.358
	Spinel-3	2.518	8.351
	Spinel-1	2.513	8.335
Canister #20	Spinel-2	2.526	8.378
	Spinel-1,3	2.515	8.341
"Dead volume"	Spinel	2.518	8.351

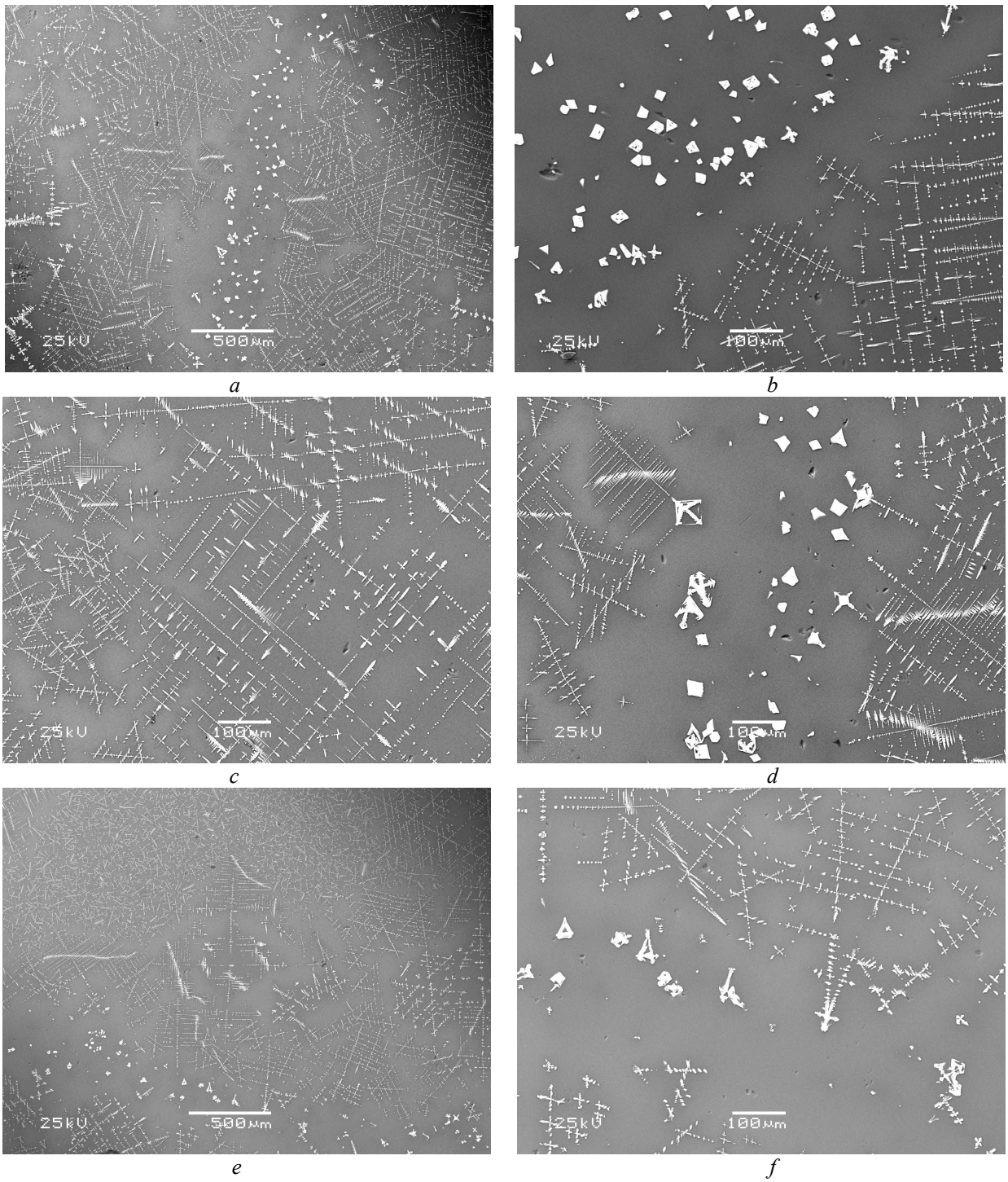

Figure 4. SEM Images of the Glassy Product from Canister #20 (a-d) and "dead volume" (e, f).

a, e – general view; b, f – border zone between zones with the skeleton-type and individual crystals; c – zone of the skeleton-type crystals; d – zone of individual crystals.

Canister #20 are more uniform in chemical composition and only two well-resolved peaks are observed on the XRD pattern. The sample from the "dead volume" cooled for the longest time in the de-energized cold crucible under much more equilibrium conditions contains spinel with

rather uniform chemical composition. As a result, the XRD peak is only slightly asymmetric with respect to its position on the angular range and the lattice parameter tends to some averaged values.

Determination of the Degree of Crystallinity

We measured the degree of crystallinity of the virified SB4 waste surrogate sampled from Canisters #6, #20 and "dead volume" of the large-scale cold crucible using their SEM images (three replicate SEM microphotographs) processed by a Corel Photo-Paint software.

The degree of crystallinity of the product sampled from Canister #6 is slightly lower than that of the product from Canister #20 and "dead volume" of the cold crucible. As expected the highest degree of crystallinity is observed in the product sampled from the "dead volume" (13.3 vol.% in the zone with the skeleton-type crystals and 10.7 vol.% in the zone with individual crystals). Average degree of crystallinity may be estimated as ~12 vol.%. This value is a little bit higher than that observed in the product obtained in the bench-scale cold crucible but at higher waste loading (60 wt.%). The degree of crystallinity of the product with ~50 wt.% waste loading obtained in smaller crucible was estimated to be ~5-7 vol.%. Slower cooling rate in larger sized cold crucible favors an increase in the degree of crystallinity and larger crystallite size.

Infra-Red Spectroscopy Study

Infra-red spectra of the vitrified SB4 waste surrogate within the range of 1600-400 cm^{-1} consist of a very strong absorption band at 850-1150 cm^{-1}, a strong band at 400-550 cm^{-1}, weaker bands at 1350-1450 cm^{-1} and 700-750 cm^{-1}, and a weak band (shoulder) at 1250-1300 cm^{-1} (Fig. 5). The bands with maxima at 1395-1410 cm^{-1} and ~1270 cm^{-1} are components of twice degenerated asymmetric valence ν_3 O—B—O vibration in the boron-oxygen triangular BO_3 units. The bands at ~720 cm^{-1} and ~655 cm^{-1} are components of twice degenerated asymmetric deformation δ_4 O—B—O vibrations [9]. The strongest band with a maximum at ~1000 cm^{-1} is due to asymmetric O—Si—O vibrations in the tetrahedral SiO_4 units. This band is normally a superposition of the bands due to O—Si—O vibrations in the SiO_4 units with various numbers of bridging oxygen ions connecting SiO_4 tetrahedra in the network: four (Q^4) – at ~1100-1150 cm^{-1}, three (Q^3) – at ~1050-1100 cm^{-1}, two (Q^2) – at ~1000-1050 cm^{-1}, one (Q^1) – at ~950-1000 cm^{-1}, and zero (Q^0) – at ~900-950 cm^{-1}. The wavenumber range of 400-550 cm^{-1} corresponds to deformation vibrations in the SiO_4 units [10,11].

Occurrence of the bands with maxima at ~1400 cm^{-1} and ~1270 cm^{-1} indicates significant fraction of trigonally coordinated boron in all the glasses studied. Position of the maximum of the strongest band due to O—Si—O vibrations at ~990-1000 cm^{-1} points to prevailing of the Q^2 and Q^1 units in the glass network. The band with a maximum at ~720 cm^{-1} is a superposition of the bands due to asymmetric deformation δ_4 O—B—O and symmetric ν_1 O—Si—O vibrations. The latter may be present in IR spectra only if symmetry of the SiO_4 units is lower than T_d (C_{3v} or C_{2v}) [10]. The Q^4 and Q^0 units have T_d symmetry whereas the Q^1 and Q^3 units have C_{3v} and the Q^2 units have C_{2v} symmetry. Taking into account low silica content in the glassy products – vitrified SB4 waste surrogate (≤44 wt.% in the vitreous phase) only minor fraction of the Q^3 units may be present, therefore, the glass network is built from rather short metasilicate chains.

Minor BO_4 tetrahedral units may be integrated in these chains. The bands due to O—B—O vibrations in the BO_4 units and Si—O—B^{IV} vibrations bonding SiO_4 and BO_4 tetrahedra are

positioned within the same range (950-1050 cm^{-1}) as O—Si—O bonds in the SiO_4 units and cannot be clearly distinguished. However, at high Al_2O_3 content in glasses boron is predominantly three-coordinated with respect to oxygen. For all the glasses studied the ψ_B factor allowing evaluating relative fractions of three- and four-coordinated boron and determined as:

$$\psi_B = \{([Na_2O]+[K_2O]+[BaO])+0,7([CaO]+[SrO]+[CdO]+[PbO])+ 0,3([Li_2O]+[MgO]+[ZnO])-[Al_2O_3]\}/[B_2O_3]$$

is lower than zero (behavior of iron in glasses is similar to that of aluminum). At this value all the boron should be three-coordinated whereas major aluminum – four-coordinated and minor – six-coordinated [12].

As follows from IR spectra, vitreous phases have similar structure in all the glassy materials at 40 to 60 wt.% SB4 waste loading. Position of the maximum in the IR spectra of the band due to O—Si—O bonds in the SiO_4 units of the glass with ~60 wt.% waste loading is slightly shifted to lower wavenumbers (~990 cm^{-1}) indicating some lower degree of connectedness of the glass network due to higher fraction of the Q^1 units with one bridging oxygen ion.

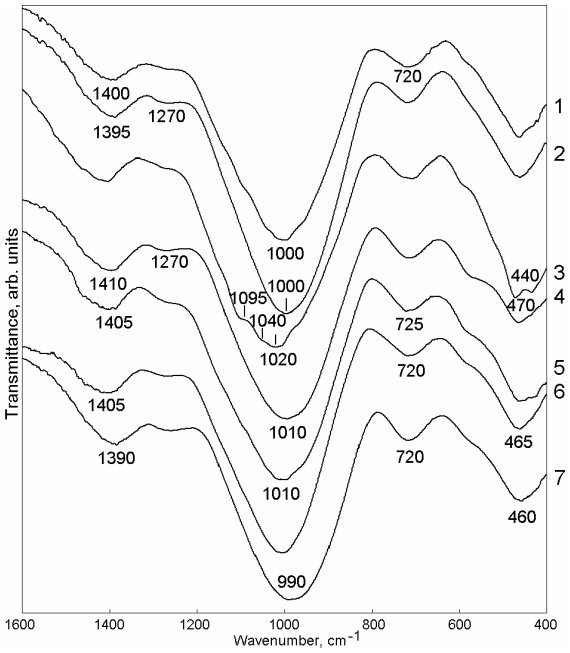

Figure 5. Infra-Red Spectra of the Glassy Materials with 40 (1,2), 50 (3-6) and 60 wt.% (7) Waste Loading Produced in the Lab- (1,3), Bench- (2,4,7), and Large-Scale (5,6) Cold Crucibles.

The bands due to vibrations of Fe^{3+}—O bonds are positioned within the ranges of 550-650 cm^{-1} (Fe^{IV}—O) and 300-400 cm^{-1} (Fe^{VI}—O) [13]. They are overlapped with strong bands due to deformation vibrations in the SiO_4 groups. Just a weak shoulder within the range 550-600 cm^{-1}, which can be attributed to vibrations of the Fe^{IV}—O in the glass network, is observed in IR spectra. Absence of narrow bands in the above-mentioned ranges indicates low content of the spinel structure phases that is consistent with XRD and SEM data.

The bands due to vibration of Al^{IV}—O bonds in the glass network are within the range of 700-850 cm^{-1} [13] and overlapped with the band due to symmetric valence vibrations in the SiO_4 units.

Leach resistance of vitrified waste

Leaching data obtained by PCT-A procedure are given in Table III to be compared with the data for the samples prepared in small crucibles in a laboratory furnace. Normalized release values for all the elements were approximately 10 to 30 times lower than those from the Environmental Assessment (EA) Standard glass and comparable to the Approved Reference Material (ARM) Standard.

It should be noted, that at the same waste loading (50 wt.%) normalized release of Li and B from the glassy material produced in the large-scale cold crucible was found to be higher by a factors of 1.5 to 2 then that from the material produced in the bench-scale cold crucible. Na and Si normalized release values from both the materials were similar. The materials from the bench-scale cold crucible were produced from chemicals simulating Frit 503-R4 whereas the materials from the large-scale cold crucible were produced from actual Frit 503-R4. It can be suggested that the lithium-borate groups maintain their structure in the final glass yielding nearly congruent release of both constituents as lithium borates.

Conclusion

Vitrification of SB4 waste surrogate at relatively low waste loading (~40 wt.%) yielded predominantly amorphous material containing traces of unreacted quartz and spinel. Increase of waste loading to 50 and, then, 60 wt.% resulted in formation of magnetite-type spinel structure phase (trevorite, zincochromite and their solid solutions). No nepheline was found even at 60 wt.% waste loading in glass. The amount of crystalline phase in the glassy materials increases with the increase of waste loading and cold crucible dimensions. Maximum content of crystalline phase in the material produced in the large-scale cold crucible was estimated to be ~12 vol.%.

Anionic motif of the glass network was built from rather short metasilicate chains with end-units having three non-bridging oxygen ions and high borate constituent with predominantly three-coordinated boron.

All the materials demonstrated low release of major elements (B, Li, Na, Si) and the release of the elements were 10 to 30 times lower than those from the Environmental Assessment (EA) Standard glass.

Acknowledgements

The work was performed under Contract between US DOE/SRNL and Daymos Ltd./SIA Radon. Authors thank Radon personnel that participated in the tests on vitrification of SB4 waste surrogate. Special thanks to Mr. K.D. Gerdes for financial support from US DOE, Ms. N.P. Penionzkiewic (SIA Radon) for recording of XRD patterns, and Mr. B.S. Nikonov (IGEM RAS) for his help in SEM/EDS study of the samples.

References

[1] S.L. Marra, R.J. O'Driscoll, T.L. Fellinger, J.W. Ray, P.M. Patel, and J.E. Occhipinti. DWPF Vitrification – Transition to the Second Batch of HLW Radioactive Sludge, *Waste Management '99. Conf.* February Tucson, AZ, ID 48-5. CD-ROM.

[2] A.P. Kobelev, S.V. Stefanovsky, O.A. Knyazev, T.N. Lashchenova, A.G. Ptashkin, M.A. Polkanov, E.W. Holtzscheiter, and J.C. Marra, Results of a 50% Waste Loading Vitrification Test Using the Cold Crucible Melter for Savannah River Site, *Waste Management '06 Conf.* February 26 – March 2, 2006. Tucson, AZ, ID 6127. CD-ROM.

[3] S.V. Stefanovsky, A.P. Kobelev, V.V. Lebedev, M.A. Polkanov, A.G. Ptashkin, O.A. Knyazev, and J.C. Marra, Cold Crucible Vitrification of Uranium-Bearing High Level Waste Surrogate, *Mat. Res. Soc. Symp. Proc. 2008* (*Scientific Basis for Nuclear Waste Management XXXI*, Sheffield, UK, 16th – 21st September 2007), Paper 5P11 (in press).

[4] S.V. Stefanovsky, A.P. Kobelev, V.V. Lebedev, M.A. Polkanov, A.G. Ptashkin, O.A. Knyazev, and J.C. Marra. Vitrification of Savannah River Site SB4 Waste Surrogate in the Radon Bench-Scale Cold Crucible Unit, *Waste Management 2008 Conf.* February 24-28, 2008. Phoenix, AZ, ID 8035. CD-ROM.

[5] A.P. Kobelev, S.V. Stefanovsky, V.V. Lebedev, M.A. Polkanov, V.V. Gorbunov, A.G. Ptashkin, O.A. Knyazev, J.C. Marra, and K.D. Gerdes. Full-Scale Cold Crucible Test on Vitrification of Savannah River Site SB4 HLW Surrogate, *The MS&T/ACerS 110th Annual Meeting*, October 5-9, 2008. Pittsburgh, PA (this volume).

[6] J.C. Marra, D.K. Peeler, T.B. Edwards, K.M. Fox, J.D. Vienna, A. Fluegel, S.V. Stefanovsky, and A.S. Aloy, Glass Formulation to Support Melter Testing to Demonstrate Enhanced High Level Waste Throughput, *Mat. Res. Soc. Symp. Proc. 2007* (*Scientific Basis for Nuclear Waste Management XXXI.* Sheffield, UK, 16th-21st September 2007), in press.

[7] American Society for Testing and Materials (ASTM). *Standard Test Methods for Determining Chemical Durability of Nuclear, Hazardous, and Mixed Waste Glasses: The Product Consistency Test (PCT)*, ASTM C1285-97, West Conshohoken, PA, 1997.

[8] S.L. Marra and C.M. Jantzen, *Characterization of Projected DWPF Glasses Heat Treated to Simulate Canister Centerline Cooling (U)*. WSRC-TR-92-142, Rev. 1, 1993. 40 p.

[9] V.A. Kolesova, Vibrational Spectra and the Structure of Alkali Borate Glasses, *Glass Physics and Chemistry* (Russ.) Vol. 12, No. 1, 1986, p. 4-13.

[10] K. Nakamoto, *Infrared Spectra of Inorganic and Coordination Compounds*, John Wiley & Sons, Inc. New York – London, 1963.

[11] J. Wong, C.A. Angell, *Glass Structure by Spectroscopy*, Marcel Dekker, Inc. New York – Basel, 1976.

[12] A.A. Appen, *Chemistry of Glass* (Russ.), Khimiya, Leningrad, 1974.

[13] I.I. Plysnina, *Infrared Spectra of Minerals*, MGU, Moscow, 1977.